Interactive comment on "Coupling slope-area analysis, integral approach and statistic tests to steady state bedrock river profile analysis" by Yizhou Wang et al.

Anonymous Referee #1

Received and published: 27 September 2016

Wang et al. combine elements of the well-known slope-area and integral approaches to solve the stream power model assuming steady state. First, they estimate a value for concavity index (m/n) using an integral approach. They then determine steepness index. They argue, based on previous work, that slope-area analysis can be used to identify substrate along a river (e.g. bedrock, alluvium). They discuss problems with slope-area analysis including differentiation of discrete and noisy data, which produces unstable results. Solving the integral problem avoids such issues. Statistical tests are performed to 'examine if residuals are independent and homoscedastic'.

I have three comments. My first comment concerns the assumption of steady state. The authors do not provide evidence that rivers analyzed are at steady state. They refer to Snyder et al. (2000), who used Merritts and Bull's (1989) eustatic correlations to determine uplift rates. Merritts and Bull's calculated uplift rates are very variable in space and time (0-4 mm/yr). Snyder et al. outline their reasons for assuming steady state (e.g. low and constant uplift rates for >100 ka south of the Jackass catchment, stable climate, profile shape; see their pg. 1254). They state that disequilibrium conditions are more likely in regions of high uplift-rate (e.g. the rivers north of 40oN in this study). Snyder et al. are circumspect in their assumption of steady state. River shape is not diagnostic of equilibrium conditions. In other places, recent work on inversion of drainage patterns for uplift rate histories indicates that river profile shapes are controlled by spatio-temporal variations in uplift rate moderated by erosional processes (e.g. Pritchard et al., 2009; Roberts & White, 2010; Roberts et al., 2012). The inverse integral approach first described in these papers does not require a priori assumption of steady state.

The assumption of steady state makes it difficult to interpret changes in concavity index reported by the authors. Perhaps the shapes of these rivers are a function of smoothly varying uplift rates and a simpler erosional history? It would be straightforward to test this idea by inverting for uplift rate histories and comparison of results to independent observations of uplift along the Californian coastline.

Thanks for the comment. River shape is not diagnostic of equilibrium conditions despite linear fit to the log-transformed slope-area data or the χ-z plot.

In the low-uplift zone (streams Hardy to Dehaven), the uplift rate has been approximately constant (rather than smoothly varying values) for at least 0.33 Ma (Merritts and Bull, 1989). The bedrock-channel reaches upstream are probably not affected by sea-level fluctuations (Snyder et al., 2000). These streams thus can be under steady state. Higher concavity values in the lower reaches may be due to sedimentation affected by sea-level fluctuations.

However, disequilibrium conditions are likely in the high-uplift zone. To test the steady assumption, we modeled uplift rate histories (see Sect. 4.2 for details).

For spatially variant rock uplift, the study area can be divided into four distinct zones, from north to south, the north transition zone (streams Singley to Cooskie), the King Range high-uplift zone (streams Randall to Buck), the intermediate-uplift zone (streams Horse Mtn), and the low-uplift zone (streams Hardy to Dehaven). Within each zone, we assumed spatially invariant rock uplift for its small drainage area. We extracted all the fluvial channels and calculated a mean χ-z plot for each zone. Base on n=1 and variable erodibility K (relates to uplift rates), we utilized a linear inversion model of Goren et al (2014) to inferred the rock uplift histories $U(t)$.

As shown by Fig. 15j, the rock uplift rates in the low- and intermediate-uplift zones have been constant (~0.3-0.4 mm/a since 0.4 Ma, and ~2-2.5 mm/a since 0.16 Ma, respectively). The north transition and high-uplift zones both experienced increases in uplift rates (from ~2.5 mm/a to 3.3 mm/a, and from ~3.7 mm/a to 4.3 mm/a, respectively) starting ~0.12 Ma ago. However, the increase ratios are much lower. The uplift rates have been constant for at least 0.12 Ma (the maximum response time is ~0.16 Ma) and no knickpoints are found along the rivers, which means that the river channels have been reshaped by the recent tectonic activity and already have reached steady state.

Secondly, there are a number of relevant papers that are not cited. For example, the integral methodology was developed in a number of papers not discussed (e.g. Pritchard et al., 2009; Roberts & White, 2010; Roberts et al., 2012; Czarnota et al., 2014; Paul et al., 2014; Wilson et al., 2014). Their results suggest that uplift can be inserted along rivers, which makes values of chi difficult to interpret. Erosional parameter values in the stream power model (e.g. m and n) can be determined from joint inversion of drainage patterns (e.g. Rudge et al., 2015). In Roberts et al. (2012, doi:10.1029/2012TC003107) the slope-area methodology was shown to produce unstable results for small amounts of randomly distributed noise.

Thanks for the comment and we have cited these papers. We cite papers (Pritchard et al., 2009; Roberts and White, 2010; Roberts et al., 2012; Czarnota et al., 2014; Paul et al., 2014; Wilson et al., 2014) in Line33, Page9.

We cite the paper (Rudge et al., 2015) in Line19 Page7.

We cite the paper (Roberts et al., 2012) in Line22 Page8. Roberts et al (2012) noticed that the slope-area methodology may produce unstable results for small amounts of randomly distributed noise. In spite of little knowledge about the elevation data uncertainty here, we utilized different datasets and various data handling methods (data smoothing and sampling) to calculate slope with different uncertainties. Then, to some extent, the influence of data uncertainty can be tested (see Sect. 4.3 for details).

In the case study, the channel slope is derived from 1 Arc-second SRTM DEM via 300 m smoothing window and 20 m contour sampling interval. Then, we reanalyzed streams in the high- and low-uplift zones based on 1/3 arc-second USGS DEM. We calculated the channel slope via various strategies: 300 m smoothing window and 20 m contour sampling interval, 300 m smoothing window and 10 m contour sampling interval, and 100 m smoothing window and 10 m contour sampling interval, respectively. We found no distinct difference is in concavity and channel steepness values derived from different datasets or data handling methods. Therefore, in this study area, uncertainty in elevation data may not cause distinct differences in parameter estimates (e.g. θ and k_{sn}).

Finally, the methodology (e.g. lines 26-30 on page 4 and lines 1-4 on page 5) is difficult to follow. I think the authors suggest that concavity indices vary along rivers with different substrates (e.g. alluvium, bedrock)? And the point of doing the slope-area analysis is to identify where substrate changes? Their approach needs to be explained more clearly. For example, I think caption to Figure 4c could be clearer (e.g. 'The correlation coefficients of chi-z plots as a function of theta for the bedrock portion of the river'). A comparison between predictions of substrate from slope-area analysis and observations would give the reader more confidence in results (e.g. page 4, lines 14 and 26-30). Can substrate be verified using, for example, satellite imagery/the Snyder paper? Some terminology used is confusing. For example, what does 'proper bedrock channel concavity' mean?

Thanks for the comment. We suggest that concavity indices vary along rivers with different substrates (e.g. alluvium, bedrock). The point of doing the slope-area analysis is to identify where substrate changes. We have revised the text (lines 1-19 on page 5) and the caption to Figure 4c (The correlation coefficients of chi-z plots as a function of θ for the bedrock portion of the river).

The substrate of the streams in the case study has been verified by Snyder et al (2000, 2003).

We have rectified the confusing terminology 'proper bedrock channel concavity' as 'concavity of the bedrock portion of the river' in Line5 Page5.

Typographical errors. Page 3, line 7: '…a better way to [perform] stream profile analysis'. Page 3, line 15: define zb. Page 4, lines 15, 27, 28: add spaces between numbers and units. Caption to Figure 4: labels for panels e and f are incorrect. Figure 4, panel (f): 'aluvial'.

Thanks for the comment and we have rectified these errors.

The coupled process does provide a better way to perform stream profile analysis (Line10, Page3).

We define z_b as the channel elevation at x=0 (river mouth). Line 7 page 2.

We have added spaces between numbers and units Page 4, lines 19; Page5 Lines 2, 3.

We have rectified the caption to Fig. 4 and the word 'alluvial' in Fig. 4f.

Interactive comment on "Coupling slope-area analysis, integral approach and statistic tests to steady state bedrock river profile analysis" by Yizhou Wang et al.

Anonymous Referee #2

Received and published: 30 September 2016

This contribution compares and combines two approaches for analyzing steady state bedrock channels, the slope-area and integral methods. It uses a well-studied set of streams in tectonically active northern California as its test case. The main finding is that the integral approach yields better-constrained values of channel concavity and steepness parameters. The slope-area method is useful to identify scaling breaks, which are then used as limits over which to apply the integral method. Given the popularity of longitudinal profile analysis in tectonic geomorphology, this kind of methods comparison has value. I have several suggestions for improving the manuscript.

1. The MTJ site is well studied, but has the disadvantage of including only short (<10 km long; <20 km2 area) streams. Choosing a site with longer, larger rivers (and therefore more robust scaling between slope or chi and area) would have some merit, given the statistical focus of the study. Longer streams would likely also show clearer downstream transitions between colluvial, bedrock and alluvial conditions. Some of the limitations of the MTJ study area for slope-area analysis where discussed by Wobus et al. (2006), but this study does not make much reference to those findings.

Thanks for the comment. The case study has disadvantages of including only short (<10 km long; <20 km^2 area) and steady streams. In many landscapes, especially large rivers, this steady assumption will not be met. Then, we took Mattole, a large river in the MTJ region, for example, to extract the unsteady signals. Here, 1/3 arc-second USGS DEM was used (see Sect. 4.4 for details).

We derived a log-transformed slope-area plot of the stem (300 m smoothing window and 20 m contour sampling interval) and recognized a knickpoint by the scaling break in the slope-area data. The knickpoint locates at the elevation of ~280 m. Concavity indices above (0.61±0.01) and below (0.58±0.07) the knickpoint are nearly the same.

Using the integral approach and two statistic tests, we derived the k_{sn} above (10.81±0.86 $m^{0.9}$) and below (17.44±1.16 $m^{0.9}$) the knickpoint. The k_{sn} values of the Mattole stem are much lower than that of the adjacent streams (e.g. Singley, Davis, Fourmile and Cooskie), suggesting that other variables (e.g. sediment flux and lithology) may affect channel steepness. This might limit our ability to quantitatively relate steepness indices to uplift rates in this field setting, as noticed by Wobus et al (2006).

Usually, the method of best linearizing χ-z plot can be used to compute θ of a steady-state bedrock channel. However, in many cases, whether a stream is under steady state is unknown. We computed the correlation coefficients between channel elevation and χ values of the stem based on a range of θ. Different from the result of slope-area analysis, the best linear fit corresponds to θ=0.30. Thus, a river may be in disequilibrium condition despite a linear relationship in the χ-z plot. Therefore, in this case, slope-area analysis might be a good choice to determine whether the river profile is under steady state, although the difference in channel substrates is unrevealed from the log-transformed slope-area data.

We calculated the map of channel steepness. The channels show low k_{sn} values along the whole stem and its tributaries (low elevation) above the knickpoint but higher values in the upstream (high elevation) of tributaries below the knickpoint. Among the tributaries in the west of the stem, channel steepness decreases from the central part (high-uplift zone) towards both north (north transition zone) and south (intermediate-uplift zone). Both the spatial pattern of k_{sn} and positive relationship between k_{sn} and elevation may indicate a tectonic control on channel steepness despite other potential variables.

2. The authors use 1 arc-second SRTM DEM, which has a very coarse resolution compared with the 1/3 arc-second DEM available from the USGS (Wobus et al., 2006). Why was the coarse dataset used? Also, how were the profile smoothing parameters chosen (e.g., Figure 3 caption)?

Thanks for the comment. In Figs. 3, 4 and 5, a method of 300 m smoothing window and 20 m contour sampling interval was chosen.

Roberts et al (2012) noticed that the slope-area methodology may produce unstable results for small amounts of randomly distributed noise. In spite of little knowledge about the elevation data uncertainty here, we want to utilize different datasets (1/3 arc-second USGS DEM and 1 arc-second SRTM DEM) and various data handling methods (smoothing window and contour sampling interval) to calculate channel slope with different uncertainties. Then, to some extent, the influence of data uncertainty can be tested (see Sect. 4.3 for details).

3. In the slope-area method of the uncertainty in steepness partially comes from the uncertainty in concavity. Different concavities result in very different steepnesses; this is the reason that researchers use a reference concavity when comparing channels. The authors do not present an uncertainty on the concavity values found via the integral approach; this may explain the extremely low uncertainties on the steepness values.

Thanks for the comment. For the integral approach, two methods are used to determine the channel concavity: 1) best linearize the χ-*z* plot of the stem; 2) maximizes the co-linearity of the main stem with its tributaries. Based on either method, we can only derive a unique concavity value (It is different with slope-area analysis).

For steady streams with uniform rock uplift rates, lithology and climate, the two kinds of θ values can be similar. The limited difference between the two values can be an uncertainty estimate of concavity. In this study, we utilized both methods to calculate the channel concavity values to see whether they are similar (e.g. Lines16-21, Page 6).

For the same stream, distinct difference in the two kinds of concavity values may suggest other potential variables, for example, unsteady channels (Lines 19-20, 30 Page 9) and variant substrates (Lines22-30, Page 6).

4. As others have done in past studies, the authors choose the part of the stream in which to conduct the analysis (the bedrock channels) based on scaling breaks in the slope-area data (Figures 3a and 4a). In the ideal case, these transitions would be mapped in the field, although in practice they are likely gradual and difficult to identify on the ground. Why do the authors believe that the scaling breaks identified in slope area data are more geomorphically meaningful than those seen in the integral analysis (e.g., Figure 4 analysis; p. 4-5)? I suspect that the authors are assigning too much geomorphic meaning to fairly subtle scaling breaks seen in the slope-area data.

Thanks for the comment. The transitions between colluvial, bedrock and alluvial portions of the channel have been verified by Snyder et al (2000, 2003). In Fig. 4, we show that concavity indices vary along rivers with different substrates (e.g. alluvium, bedrock). The variation in θ can be seen directly in the slope-area plot.

We do not mean that the scaling breaks identified in slope-area data are more geomorphically meaningful than those seen in the integral analysis. In fact, they are with different geomorphically meanings.

In Fig.4, the scaling break identified in slope-area data shows difference in channel concavity values. Usually, channel concavity is more related to lithology than channel steepness.

The scaling break in χ-z plot shows difference in channel steepness rather than concavity indices. This is useful to extract the rock uplift history (In Sect. 4.2, we modeled the uplift histories based on the χ-z plots of the streams).

Coupling slope-area analysis, integral approach and statistic tests to steady state bedrock river profile analysis

Yizhou Wang, Huiping Zhang, Dewen Zheng, Jingxing Yu, Jianzhang Pang, and Yan Ma

State Key Laboratory of Earthquake Dynamics, Institute of Geology, China Earthquake Administration, Beijing 100029, China

Correspondence to: Yizhou Wang (wangyizhou.-123@163.com)

Abstract. Slope-area analysis and the integral approach both have been widely used in stream profile analysis. However, channel steepness derived from the former one is characterized by large uncertainties and deviated concavities, and false knickpoints may occur when utilizing the integral approach. Limited work has been done to couple the advantages of the two methods and to remedy such drawbacks. Here we show the merit of the log-transformed slope-area plot to identify colluvial, bedrock and alluvial channels along river profiles. Via the integral approach, we manage to obtain bedrock channel concavity and steepness with high precision. In addition, we run bi-variant linear regression statistic tests for the two methods to examine and eliminate serial correlation of residuals. We finally suggest that, the coupled process, integrating the advantages of both slope-area analysis and the integral approach, can be a more robust and capable method for bedrock river profile analysis.

1 Introduction

In an evolving landscape, information about tectonics, climatic change, and lithology can be recorded by the bedrock river profiles (Fox et al., 2014, 2015; Goren et al., 2014; Harkins et al., 2007; Royden and Perron, 2013; Snyder et al., 2000). How to retrieve such details has long been a focus in both geologic and geomorphologic researches (Flint, 1974; Wobus et al., 2006; Rudge et al., 2015). Most of these studies are based on a well known power-law relationship between local channel gradient and drainage area (Flint, 1974; Hack, 1973; Howard and Kerby, 1983):

$$\frac{dz}{dx} = k_s A^{-\theta} \quad (1)$$

$$k_s = (U/K)^{1/n} \quad (2)$$

$$\theta = m/n \quad (3)$$

where z is elevation, x is horizontal upstream distance, U is bedrock uplift rate, K is an erodibility coefficient, A is drainage area, and m and n are constants. Parameters θ and k_s are referred to as concavity and steepness indices, respectively. The power-law scaling holds only for drainage areas above a critical threshold, A_{cr}, which is the transition from divergent to convergent topography or from debris-flow to fluvial processes (Montgomery and Foufoula-Georgiou, 1993; Tarboton et al., 1989; Wobus et al., 2006). A growing number of studies have quantitatively related steepness to rock uplift (Hu et al., 2010;

Kirby and Whipple, 2012; Kirby et al., 2003, 2007; Tarboton et al., 1989). Assuming a steady state river profile under constant rock uplift rates and erodibility in time and space, two forms of solutions to Eq. (1) are derived:

$$\log\left(\frac{U}{K}\right)^{1/n} + \left(-\frac{m}{n}\right)\log A = \log\left(\frac{dz}{dx}\right) \quad (4)$$

$$z = z_b + \left(\frac{U}{KA_0^m}\right)^{1/n}\chi \quad (5)$$

$$\chi = \int_0^x \left(\frac{A_0}{A(x')}\right)^{m/n} dx' \quad (6)$$

where z_b is the channel elevation at x=0 (river outlet). This is a boundary condition to Eq. (1). A_0 is an area-scale factor.

The slope-area analysis, as shown in Eq. (4), yields concavity and steepness indices by a linear fit to log-transformed slope and area data. This makes it convenient to discriminate different channel substrates from concavity indices. For example, available studies indicate that the colluvial, bedrock and alluvial channels can be directly identified from the log-transformed slope-area plot (Kirby et al., 2007; Snyder et al., 2000, 2003; Wobus et al., 2006). However, for its need to estimate slope by differentiating and resampling noisy elevation data, considerable scatter will be typically caused in slope-area plots, making it challenging to identify a power-law trend with adequate certainty (Perron and Royden, 2013). What's more, the derived channel steepness is doomed to be with high uncertainty due to error propagation (see Sect. 3 for details).

The integral approach, based on an integration of Eq. (1), was proposed by Royden et al (2000) to alleviate such problems by avoiding calculating channel slope. As shown in Eqs. (5) and (6), the transformed variable χ can be determined directly from drainage area data by simple numerical integration. Based on a proper concavity, the steady state river profile can be converted into a straight line. Slope of the line is steepness (we assume A_0=1 m^2 throughout the paper). As the best fit value of θ is not known a priori, we can compute χ-z plots for a range of θ values and test for linearity (Perron and Royden, 2013). Thus, this method provides an independent constraint on both θ and k_s (Perron and Royden, 2013). Nevertheless, the uncertainty in k_s will be underestimated for serially correlated residuals. In addition, we may get false concavities and knickpoints for its weakness to identify the channel types (see Sect. 3 for details).

Based on the analysis above, coupling the advantages of the two methods can make up for their individual drawbacks and provide a better way to constrain stream power parameters. We also run bivariate linear regression statistic tests for the two methods to evaluate if the residuals of linear fit are homoscedastic and serially correlated. In this paper, we take streams, located in the Mendocino Triple Junction (MTJ) region of northern California (Fig.1), for example, to illustrate the process.

2 Methods

2.1 Coupling slope-area analysis and the integral approach

A natural river usually consists of different channel substrates, for example, colluvial, bedrock and alluvial channels. In spite of their complex formation processes, we can identify them from a log-transformed slope-area plot (Fig. 1) (Snyder et al., 2000). The colluvial channel, characterized by steep channel slope (>20^o) and limited drainage area (<A_{cr}) (Wobus et al., 2006), is debris-flow-dominated and beyond the capability of Eq. (1). Both bedrock (detachment-limited) and alluvial (transport-limited) channels show descending gradient with increasing drainage areas, which often exhibit a power-law scaling. However, the alluvial channel is often characterized by much gentler gradient and a higher concavity (Kirby et al., 2007; Snyder et al., 2000; Whipple and Tucker, 2002), which can be distinguished in the log-transformed plot (Fig. 1).

Via the integral approach (Perron and Royden, 2013), we could get concavities of bedrock channels. Based on a reference concavity index (Hu et al., 2010; Kirby et al., 2003, 2007; Perron and Royden et al., 2013; Snyder et al., 2000;Wobus et al., 2006), we then derived the normalized channel steepness indices subject to lower uncertainties.

2.2 Statistic tests

The coupled process does provide a better way to perform stream profile analysis. However, little has been done to work on the statistic tests of either slope-area analysis or the integral approach. Perron and Royden (2013) noticed the influence of auto-correlated residuals on the steepness uncertainty. In addition, we should make sure that the variance of residuals is a constant (homoscedastic) (Cantrell, 2008; Kirchner, 2001). Here, we introduced Durbin-Watson test (Durbin and Watson, 1950) and Spearman rank correlation coefficient test (Choi, 1977; Fieller et al., 1957; York, 1968) to examine if the residuals are independent and homoscedastic.

2.2.1 Durbin-Watson test

We took the integral approach for an example and rewrote Eq. (5) into another form:

$$z_i = z_b + k_s\chi_i + e_i \ (i = 1, 2 \cdots p) \tag{7}$$

In the formula, p is the number of elevation data points, and e represents residuals. We determined the Durbin-Watson (DW) statistics in the following steps:

1) We first calculated the self-correlation coefficient of residuals via Eq. (8):

$$r = \frac{\sum_{i=2}^{p} e_i e_{i-1}}{\sqrt{\sum_{i=2}^{p} e_i^2}\sqrt{\sum_{i=2}^{p} e_{i-1}^2}}, \tag{8}$$

2) Then, the DW statistic was derived as: DW=2×(1-r). Since -1≤r≤1, DW falls in the range of 0-4.

3) We then examined if the residuals were auto-correlated according to Table 1.

To eliminate the self-correlation, new variables were generated as Eq. (9):

$$z_i' = z_i - r z_{i-1}, \ \ \chi_i' = \chi_i - r\chi_{i-1} (i = 1,2 \cdots p), \tag{9}$$

Slope of a linear fit to revised relative elevation, z', and χ'data are channel steepness.

2.2.2 Spearman rank correlation coefficient test

To evaluate if the variance of residuals is a constant, we utilized Spearman rank correlation coefficient test (Choi, 1977; York, 1968):

1) Via a linear regression of χ-z plots, we derived the absolute values of residuals $|e|$;

2) We sorted the χ values in descending order and recorded the ranks $d_{i\text{-}1}$. Then the χ values were sorted again according to $|e|$ and the new ranks were recorded as $d_{i\text{-}2}$;

3) The Spearman rank correlation coefficient, rs, and the t-statistics, t, were calculated via Eqs. (10) and (11):

$$rs = 1 - \frac{6}{p(p^2-1)} \sum_{i=1}^{p} (d_{i-1} - d_{i-2})^2 \qquad (10)$$

$$t = \frac{\sqrt{p-2}}{\sqrt{1-rs^2}} rs \quad (i = 1,2 \cdots p) \qquad (11)$$

4) When the t value is lower than a threshold, $t_{\alpha/2}$ (p-2), the variance of residuals is a constant. In our example, with $p > 30$ and significance level $\alpha = 0.05$, the threshold value is larger than 2.58.

3 Case study: Mendocino Triple Junction (MTJ) region

Based on 1 arc-second SRTM DEM (digital elevation model), we extracted 15 streams in Mendocino Triple Junction (MTJ) region (Fig. 2). Here we first took streams Cooskie and Juan, for example, to illustrate the advantages and disadvantages of slope-area analysis and the integral approach, as well as to explain the reason of coupling the two methods.

Channel concavity and steepness indices can be derived from either slope-area analysis or the integral approach. For the same river profile, both methods should yield identical results (Harkins et al., 2007). We divided the profile of Cooskie stream into colluvial and bedrock channels from the log-transformed slope-area plot (Fig. 3a). The elevation and area of the dividing point are ~500 m (Fig. 3b) and 0.1 km^2 (critical area, A_{cr}). The concavity of bedrock channel is ~0.47±0.05. We also computed the correlation coefficients between bedrock channel elevation and χ values based on a range of θ values. The best linear fit corresponds to θ=0.45. Both of them are similar to the result (0.43±0.12) of Snyder et al (2000), but slightly higher than the result (0.36) of Perron and Royden (2013), which may be attributed to the difference in DEM resolution or choosing different critical areas.

Although the concavities derived from the two methods are in agreement with each other, uncertainties in channel steepness differ a lot. The uncertainty from slope-area analysis is ~40% (k_s=79.16±29.35) (Fig. 3a), but the integral approach gives only ~0.5% (k_s=62.81±0.39) (Fig. 3d). In addition to smoothing and re-sampling of elevation data, we attribute such large uncertainty to error propagation. The natural logarithmic value of steepness from slope-area analysis is 4.37±0.37, which results in a k_s value of 79.16±29.35. This indicates that the steepness indices will have large uncertainties even for high linear correlation of the log-transformed slope-area plot. Hence, the integral approach is much better for calculating channel steepness.

Concavity indices usually vary along river channels where different substrates outcrop (e.g. alluvium, and bedrock). For example, along the Juan River, we identified colluvial (drainage area<0.16 km^2, elevation>700 m), bedrock and alluvial (drainage area>8.89 km^2, elevation<150 m) channels from the log-transformed slope-area plot (Figs. 4a and b). As shown in Fig. 4a, these channels are characterized by different concavities, consistent with estimates from Snyder et al (2000). According to the concavity of the bedrock portion of the river (θ=0.52, derived from the integral approach, Fig. 4c), the bedrock channel profile is converted into a straight line (Fig. 4d).

Nevertheless, for the integral approach, it is difficult to recognize bedrock and alluvial channels along a river profile. When computing χ-z plots (A_{cr}=0.16 km^2, for the whole fluvial channel including both bedrock and alluvial portions) based on a series of concavity values, the best fit θ is 0.72 (Fig. 4e). As shown by the transformed profile (Fig. 4f), a knickpoint (at elevation of ~400 m) occurs on the channel. Below the knickpoint, the alluvial and bedrock portions share the same slope (k_s=3354±20 m$^{1.44}$) despite the different channel substrates. Above the knickpoint, the k_s value is 1667±15 m$^{1.44}$. Variations in the slope of χ-z plot may be treated as spatially or temporarily variant rock uplift rates (Goren et al., 2014; Perron and Royden, 2013; Royden and Perron, 2013). However, stream Juan is under steady state (Snyder et al., 2000; see Sect. 4.2 for discussion). Since stream power parameters will be misunderstood when using the integral approach alone, we should couple the two methods for river profile analysis.

According to the log-transformed slope-area plots, we identified bedrock channels of the 15 streams. Concavity indices were then calculated via both slope-area analysis and the integral approach. As shown in Fig. 5, both methods yielded similar concavities. Based on a mean θ value of 0.45±0.10 (1σ), we computed χ-z plots and normalized steepness indices (k_{sn}) with uncertainty estimates (Fig. 6).

We run statistic tests (Durbin-Watson test and Spearman rank correlation coefficient test) for the integral approach and slope-area analysis. For the integral approach, all the DW statistics are lower than D_L (Fig. 7a), indicating serially correlated residuals. Then, we revised the elevation and χ data according to Eq. (9) (Fig. 8). The DW statistics of revised χ-z plots are all between D_U and 4-D_U (Fig. 7a), indicating independent residuals. The results of linear fit are shown in Fig. 8. Although the revised steepness values are similar to the former, estimates of uncertainty are nearly four times to previous ones. For slope-area analysis, the DW statistics are all between D_U and 4-D_U (Fig. 7b), showing no auto-correlation.

We also calculated t-statistics for both slope-area analysis and the integral approach (Figs. 7a and b). All the results are less than 2, indicating homoscedastic residuals.

In addition to statistic tests, another way proposed by Perron and Royden (2013) to estimate uncertainty in steepness is to make multiple independent calculations of different river profiles. From Fig. 6, the mean k_{sn} of high uplift zone (U=4 mm/yr) is 104.40±14.06, and that of low uplift zone (U=0.5 mm/yr) is 71.25±10.08. The standard errors of the mean k_{sn} among profiles are considerably larger than that for individual streams. However, for multiple profiles under similar geological and/or climatic settings, this approach should provide more meaningful estimates of uncertainty.

4 Discussion

Slope-area analysis is useful to identify difference in substrates along a river (e.g. bedrock, alluvium), which can be used as regression limits to apply the integral method. The integral approach yields better-constrained values of θ and k_{sn}. Combining them and statistic tests, this coupled approach thus provides more reliable results while applied to perform stream profile analysis. In the following sections, we will discuss the parameter uncertainty and steady assumption to better illustrate this method.

4.1 Uncertainty of channel concavity

Perron and Royden (2013) noticed that the concavity uncertainty resulted from slope-area analysis described how precisely one can measure slope rather than the precision of parameters known for a given landscape. They suggested that the difference between θ values that best linearize the main stem profile and that maximize the co-linearity of the main stem with its tributaries could be an estimate of uncertainty in θ for an individual drainage basin.

In most cases, the θ value that collapses the main stem and its tributaries is often used as a reference concavity (Perron and Royden, 2013; Willett et al., 2014; Yang et al., 2015). In fact, supposing a drainage basin under uniform geologic and climatic settings, this kind of θ value can be compared with the mean value of concavities of the stem and its tributaries. We thereafter, name these two concavities θ_{Co} and θ_{mR}, respectively.

We extracted the stems and tributaries of streams, Singley, Davis, Fourmile and Cooskie (Fig. 9a), based on A_{cr} of 0.1-0.16 km^2 (Fig. 5). We calculated the correlation coefficients of χ-z plots based on a range of θ (Figs. 9b-d). The θ_{mR} of catchments are 0.45, 0.48, 0.43, and 0.55. We also derived θ_{Co} which collapses the stem and tributaries, 0.45, 0.45, 0.45, and 0.55 (Fig. 10). Both θ_{Co} and θ_{mR} are similar to the stem concavities, 0.50, 0.42, 0.50, and 0.45 (Fig. 5). Hence, for steady state bedrock channels under uniform lithologic and climatic settings, all three kinds of concavities should be similar. Then, the difference between these θ values could be an estimate of concavity uncertainty.

However, it is different for streams consisting of both bedrock and alluvial channels. We extracted the stems and tributaries of streams, Hardy, Juan, Howard and Dehaven (Fig. 11a). The θ_{mR} values of them are 0.57, 0.68, 0.73, and 0.73 (Figs. 11b-e), similar to the stem concavities (0.63, 0.70, 0.72, and 0.75) (Figs. 11b-e), but larger than the θ_{Co} (0.45, 0.45, 0.45, and 0.55) (Fig. 12). In such case, differences between θ_{Co} and θ_{mR} are not random errors and cannot be estimates of concavity uncertainty.

Nevertheless, θ_{Co} values (0.45, 0.45, 0.45, and 0.55) are similar to the concavities of bedrock reaches of stems (0.55, 0.52, 0.55, and 0.40) (Fig. 5). Then, the differences between θ_{Co} and concavities of bedrock reaches may be estimates of uncertainties in θ. Hence, the reference concavity collapsing the stem and its tributaries works well even for complex channels consisting of both bedrock and alluvial channels.

In most cases, a somewhat higher constant critical area (e.g. 1 or 5 km^2) is assumed to calculate χ values of fluvial channels (Goren et al., 2014, 2015; Willett et al., 2014; Yang et al., 2015). Here we extracted streams of four drainages (Fig. 13a), Hardy, Juan, Howard, and Dehaven, based on a critical area of 0.5 km^2 (three or four times the actual values). We then derived the concavities that best linearize stems (0.73, 0.78, 0.82, and 0.84) (Figs. 13b-e), θ_{mR} (0.60, 0.80, 0.75, and 0.75) (Figs. 13b-e), and θ_{Co} (0.40, 0.50, 0.45, and 0.55) (Fig. 14), respectively. All the results are similar to those based on actual critical areas (Figs. 11 and 12). Hence, choosing a uniform A_{cr} somewhat different to the actual values might be reasonable and would not have significant influence.

4.2 Steady state assumption of streams in the MTJ region

Usually, river shape may not be diagnostic of equilibrium conditions. In some places, recent work on inversion of drainage patterns for uplift rate histories indicates that river profile shapes are controlled by spatio-temporal variations in uplift rate moderated by erosional processes (Pritchard et al., 2009; Roberts and White, 2010; Roberts et al., 2012).

In the MTJ region, the uplift rates determined by marine terraces are variable in space and time (0-4 mm/a, Merritts and Bull, 1989). However, in the low-uplift zone (streams Hardy to Dehaven), uplift rates have been approximately constant for at least 0.33 Ma (Merritts and Bull, 1989). The bedrock-channel reaches are probably not affected by sea-level fluctuations (Snyder et al., 2000). These streams thus can be in or near equilibrium. Nevertheless, disequilibrium conditions are likely in regions of high-uplift rate (e.g. the rivers north of 40°N). To test the steady state assumption, we modelled the uplift rate histories.

Erosional parameters in the stream power model (e.g. m and n) and uplift histories can be determined from joint inversion of drainage network (Glotzbach 2015; Goren et al., 2014; Pritchard et al., 2009; Rudge et al., 2015). Here, we utilized the method of Goren et al (2014). For spatially variant rock uplift, the study area is divided into four distinct zones, from north to south, the north transition zone (streams Singley to Cooskie), the King Range high-uplift zone (streams Randall to Buck), the intermediate-uplift zone (stream Horse Mtn), and the low-uplift zone (streams Hardy to Dehaven) (Figs. 15a-d; Snyder et al., 2000). Within each zone, we assumed spatially invariant rock uplift for small drainage areas and similar uplift rates determined from marine terraces (Merritts and Bull, 1989). Snyder et al (2000) suggested n~1 and variable K between the high- and low-uplift zones. According to the linear inversion model of Goren et al (2014), the present river channel elevation is determined by both rock uplift rate and response time, $\tau(x)$ (time for perturbations propagating from the river outlet, at x=0, to a point x along the channel):

$$z(x) = \int_{-\chi(x)}^{0} U^*(t^*)\, dt^* \tag{12}$$

$$U^* = U/(KA_0^m), \;\; t^* = KA_0^m t \tag{13}$$

For the linear model (n=1) and A_0=1 m^2, response time $\tau(x)=\chi(x)/K$. The scaled time t^* has the same unit of χ, and U^* is dimensionless rock uplift rate.

Since χ-z plot may be affected by other factors (e.g., climate and lithology), we extracted all the fluvial channels and calculated a mean χ-z plot for each zone (Figs. 15e-h). We defined z_1, z_2, ..., z_N and χ_1, χ_2, ..., χ_N to be the elevations and χ values of N data points along a fluvial channels network (N=10 here). Then, based on Eq. (12), the dimensionless rock uplift histories for the four zones are shown in Fig. 15i. For the low-uplift zone, alluvial channels in the lower reaches were excluded for them being affected by sea-level fluctuations.

We utilized various erodibility ($K=U/k_{sn}$) values to calculated rock uplift rates. The K values for transition, high-uplift, intermediate and low-uplift zones are 6.17×10^{-5} $m^{0.1}$/a, 3.82×10^{-5} $m^{0.1}$/a, 3.38×10^{-5} $m^{0.1}$/a, and 0.37×10^{-5} $m^{0.1}$/a, respectively. According to the inferred uplift histories (Fig. 15j), the maximum response time (the perturbations migrating from the river outlet to water head) differs significantly from low- (0.43 Ma) to high-uplift (0.16 Ma) zones. The rock uplift rates in the low- and intermediate-uplift zones have been constant (~0.3-0.4 mm/a since 0.4 Ma, and ~2-2.5 mm/a since 0.16 Ma, respectively). The north transition and high-uplift zones both experienced increases in the uplift rates (from ~2.5 mm/a to 3.3 mm/a, and from ~3.7 mm/a to 4.3 mm/a, respectively) starting about 0.12 Ma ago. However, the increase ratios are much lower. Considering the maximum response time (~0.16 Ma), the uplift rates have been constant for a relatively long period. In addition, no large knickpoints are found along the rivers. All of these indicate that the rivers have been reshaped by the recent tectonic activities and have reached steady state.

In the recent 0.02 Ma, the rock uplift rates seem to be a bit lower (Fig. 15j). That may be due to variant channel concavities. The reaches downstream are usually characterized by rapidly decreasing gradient (higher concavities). Then, lower U^* will be produced when using a reference concavity (0.45). As a result, the modelled rock uplift rates will be low. The variance in channel concavity may indicate difference in river substrate (e.g. sedimentation affected by sea-level fluctuations) rather than tectonics (Snyder et al., 2000).

4.3 Influence of elevation data uncertainty

Roberts et al (2012) noticed that the slope-area methodology might produce unstable results for small amounts of randomly distributed noise. In spite of little knowledge about the elevation data uncertainty here, we utilized different datasets and various data handling methods (data smoothing and sampling) to calculate channel slope with different uncertainties. Then, to some extent, the influence of data uncertainty can be tested.

In the analysis above, the channel slope is derived from 1 arc-second SRTM DEM via 300 m smoothing window and 20 m contour sampling interval. Then, we reanalysed the streams in high- and low-uplift zones based on 1/3 arc-second USGS DEM (downloaded from https://catalog.data.gov/dataset/national-elevation-dataset-ned-1-3-arc-second-downloadable-data-collection-national-geospatial). We calculated the channel slope via 300 m smoothing window and 20 m contour sampling interval (Figs. 16a and d), 300 m smoothing window and 10 m contour sampling interval (Figs. 16b and e), and 100 m smoothing window and 10 m contour sampling interval (Figs. 16c and f), respectively. To get average values, streams in the same zone were composited.

We chose 0.1-3 km^2 as regression limits for the high-uplift zone and 0.2-8 km^2 for the low-uplift area. The channel concavity and steepness (k_{sn}) were calculated by linear regressing the log-transformed slope-area data and χ-z plots (θ_{ref}=0.45), respectively. The stream concavity indices in the high-uplift zone (0.41±0.05) and low-uplift region(0.48±0.03) are similar to or within error of the estimates reported by this study (0.45±0.10, 1 Arc-second SRTM DEM), Wobus et al (2006) (0.57±0.05, 10-m-pixel USGS DEM), and Snyder et al (2000) (0.43±0.11, 30 m USGS DEM). All the error estimates are characterized by 1σ. Mean k_{sn} values of 109 and 60 $m^{0.9}$ in the high- and low-uplift zones, respectively, yield a ratio of k_{sn}(high)/k_{sn}(low) of ~1.82, which is a principal conclusion upheld by both Snyder et al (2000) and Wobus et al (2006). Then, no distinct difference is found in concavity and channel steepness indices when using different datasets and data handling methods. Therefore, in this study area, uncertainty in elevation data may not cause distinct differences in parameter estimates (e.g. θ and k_{sn}).

4.4 Disequilibrium circumstances in large rivers

The case study has disadvantages of including only short (<10 km long; < 20 km^2 area) and steady streams. In many landscapes, especially large rivers, this steady assumption will not be met (Harkins et al., 2007; Wobus et al., 2006; Yang et al., 2014). Then, we took Mattole, a large river in the MTJ region (Fig. 17a), for example, to extract the unsteady signals. Here, 1/3 arc-second USGS DEM was used.

Using 300 m smoothing window and 20 m contour sampling interval, we derived a log-transformed slope-area plot of the stem (Fig. 17b). We found the critical threshold of drainage area, A_{cr}, ~0.1 km^2 and at the elevation of ~450 m (Figs. 17b and c). A knickpoint was detected by the scaling break in the slope-area data and then marked in the shaded-relief map (Fig. 17a) and the river profile (Fig. 17c). The knickpoint locates at the elevation of ~280 m. The concavity indices above (0.61±0.01) and below (0.58±0.07) the knickpoint are nearly the same. To compare with the adjacent streams, a reference concavity θ_{ref}=0.45 was used to calculate the channel steepness. Using the integral approach and two statistic tests, we derived the k_{sn} above (10.81±0.86 $m^{0.9}$) and below (17.44±1.16 $m^{0.9}$) the knickpoint. However, in the adjacent streams, (e.g. Davis, Fourmile), the k_{sn} values are much larger than 60 $m^{0.9}$. In addition to spatial variations in Holocene uplift rates of marine platforms (Merritts, 1996), it suggests that other variables (e.g. sediment flux and lithology) may affect channel steepness. This might limit our ability to quantitatively relate steepness indices to uplift rates in this field setting, as noticed by Wobus et al (2006).

Usually, the method of best linearizing χ-z plot is used to compute θ for a steady state bedrock river profile (Perron and Royden, 2013). However, in many cases, whether a stream is in equilibrium is unknown. We computed the correlation coefficients between the channel elevation and χ values (A_{cr}=0.1 km^2, A_0=1 m^2) of the stem based on a range of θ (Fig. 17d). The best linear fit corresponds to θ=0.30 (k_s=1.45±0.06 $m^{0.6}$, R=0.985, Fig. 17e), which is distinctly different from the result of slope-area analysis. Thus, a river may be in disequilibrium condition despite a linear relationship in the χ-z plot. In some cases, uplift can be inserted along rivers, which makes values of χ difficult to interpret (Czarnota et al.,2014;Paul et al., 2014;Pritchard et al., 2009; Roberts and White, 2010; Roberts et al., 2012; Wilson et al., 2014). Therefore, in this case, slope-area analysis might be a good choice to determine whether the river profile is under steady state, although the difference in channel substrates is unrevealed from the log-transformed slope-area data.

We extracted all the tributaries of the Mattole river and calculated their χ-*z* plots based on a range of θ values (Figs. 18a-d). The elevation scatters of the χ-*z* plots are plotted against θ values (Fig. 18e). The θ value that collapses the main stem and its tributaries is 0.45, showing the reasonability of using 0.45 as a reference concavity to calculate the stem k_{sn}. As shown by Fig. 18c, the knickpoint (with an elevation of about 280 m) can also be detected from the χ-*z* plot of the stem.

Based on θ_{ref}=0.45, we calculated the map of channel steepness with an elevation interval of 100 m. The channel steepness values range from 1 to 273. As shown in Fig. 19, the lower k_{sn} values are along the whole stem and its tributaries (low elevation) above the knickpoint while higher values are along the upstream (high elevation) of tributaries below the knickpoint. Among the tributaries in the west of the stem, channel steepness decreases from the central part (near streams Big to Shipman, high-uplift zone) towards both north (close to stream Fourmile, north transition zone) and south (near streams Horse Mtn and Telegraph, intermediate-uplift zone). Both the spatial pattern of k_{sn} and the positive relationship between k_{sn} and elevation may indicate a tectonic control on channel steepness despite other potential variables.

5Conclusion

In this contribution, we coupled the advantages of slope-area analysis and the integral approach to steady state bedrock river profile analysis. First, we identified colluvial, bedrock and alluvial channels from a log-transformed slope-area plot. Utilizing the integral approach, we then derived concavity and steepness indices of a bedrock channel. Finally, via Durbin-Watson statistic test, we examined and eliminated serial correlation of linear regression residuals, which produced more reliable and robust estimates of uncertainties in stream power parameters.

Acknowledgement

We thank Dr. Eric Kirby (Oregon State University) and Dr. Liran Goren (Ben-Gurion University of the Negev) for significant suggestions on slope-area analysis and the integral approach, respectively. We thank Amanda (Oregon State University) and Qi Ou (University of Cambridge) for revision in English writing. We are grateful for the grants from the National Science Foundation of China (41622204, 41272215, 41272196, 41590861, 41661134011), State Key Laboratory of Earthquake Dynamics (LED2014A03) and the Strategic Priority Research Program of the Chinese Academy of Sciences (XDB03020200). YW is also funded by state special supporting plan.

References

Cantrell, C. A.: Technical Note: Review of methods for linear least-squares fitting of data and application to atmospheric chemistry problems, Atmos. Chem. Phys., 8, 5477–5487, doi:10.5194/acp-8-5477-2008, 2008.

Champagnac, J.-D., Molnar, P., Sue, C., and Herman, F.: Tectonics, climate, and mountain topography, J. Geophys. Res., 117, B02403, doi: 10.1029/2011JB008348, 2012.

Choi, S. C.: Tests of Equality of Dependent Correlation Coefficients, Biometrika, 64, 645–647, doi:10.1093/biomet/64.3.645, 1977.

Czarnota, K., Roberts, G. G., White, N. J., and Fishwick, S.: Spatial and temporal patterns of Australian dynamic topography from River Profile Modeling, J. Geophys. Res. Solid Earth, 119, 1384–1424, doi:10.1002/2013JB010436, 2014.

Durbin, J., and Watson, G. S.: Testing for Serial Correlation in Least Squares Regression: I, Biometrika, 37, 409-428, doi: 10.2307/2332391, 1950.

Fieller, E. C., Hartley, H. O., and Pearson, E. S.: Tests for rank correlation coefficients. I, Biometrika, 44: 470–481, doi:10.1093/biomet/44.3-4.470, 1957.

Flint, J. J.: Stream gradient as a function of order, magnitude, and discharge, Water Resour. Res., 10, 969-973, doi: 10.1029/WR010i005p00969, 1974.

Fox, M., Bodin, T., and Shuster, D. L.: Abrupt changes in the rate of Andean Plateau uplift from reversible jump Markov Chain Monte Carlo inversion of river profiles, Geomorphology, 238,1-14, doi:10.1016/j.geomorph.2015.02.022, 2015.

Fox, M., Goren, L., May, D. A., and Willett, S. D.: Inversion of fluvial channels for paleorock uplift rates in Taiwan, J. Geophys. Res.-Earth, 119, 1853–1875, doi:10.1002/2014JF003196, 2014.

Glotzbach, C.: Deriving rock uplift histories from data-driven inversion of river profiles, Geology, 43, 467-470, doi:10.1130/G36702.1, 2015.

Goren, L., Castelltort, S., and Klinger, Y.: Modes and rates of horizontal deformation from rotated river basins: Application to the Dead Sea fault system in Lebanon, Geology, 43, 843–846.doi:10.1130/G36841.1, 2015.

Goren, L., Fox, M., and Willett S. D.: Tectonics from fluvial topography using formal linear inversion: Theory and applications to the Inyo Mountains, California, J. Geophys. Res.-Earth, 119, 1651–1681, doi: 10.1002/2014JF003079, 2014.

Hack, J. T.: Stream profile analysis and stream-gradient index, Jour. Research U.S. Geol. Survey, 1, 421-429, 1973.

Harkins, N., Kirby, E., Heimsath, A., Robinson, R., and Reiser, U.: Transient fluvial incision in the headwaters of the Yellow River, northeastern Tibet, China, J. Geophys. Res., 112, F03S04, doi:10.1029/2006JF000570, 2007.

Howard, A. D., and Kerby, G.: Channel changes in badlands, Geol. Soc. Am. Bull., 94, 739-752, 1983.

Hu, X., Pan, B., Kirby, E., Li, Q., Geng, H., and Chen, J.: Spatial differences in rock uplift rates inferred from channel steepness indices along the northern flank of the Qilian Mountain, northeast Tibetan Plateau, Chin. Sci. Bull., 55, 3205-3214, 2010.

Kirby, E., and Whipple, K. X.: Expression of active tectonics in erosional landscapes, J. Struct. Geol., 44,54-75, doi: 10.1016/j.jsg.2012.07.009, 2012.

Kirby, E., Johnson, C., Furlong, K., and Heimsath, A.: Transient channel incision along Bolinas Ridge, California: Evidence for differential rock uplift adjacent to the San Andreas fault, J. Geophys. Res., 112, F03S07, doi:10.1029/2006JF000559, 2007.

Kirby, E., Whipple, K. X., Tang, W., and Chen, Z.: .Distribution of active rock uplift along the eastern margin of the Tibetan Plateau: inferences from bedrock river profiles, J. Geophys. Res.,108, 2217-2240, doi:10.1029/2001JB000861, 2003.

Kirchner, J. W.: Data Analysis Toolkit #11: Serial Correlation, Course Notes from EPS 120: Analysis of Environmental Data. University of California: Berkeley, CA, available at: http://seismo.berkeley.edu/~kirchner/eps_120/EPSToolkits.htm [20 May 2012], 2001.

Merritts, D. J.: The Mendocino triple junction: Active faults, episodic coastal emergence, and rapid uplift, J. Geophys. Res., 101, 6051–6070, 1996.

Merritts, D., and Bull, W. B.: Interpreting Quaternary uplift rates at the Mendocino triple junction, northern California, from uplifted marine terraces, Geology, 17, 1020–1024, 1989.

Montgomery, D. R., and Foufoula-Georgiou, E.: Channel network source representation using digital elevation models, Water Resour. Res., 29, 3925-3934, 1993.

Paul, J. D., Roberts, G. G., and White, N.: The African landscape through space and time, Tectonics, 32, doi:10.1002/2013TC003479, 2014.

Perron, J. T., and Royden, L. H.: An Integral Approach to Bedrock River Profile Analysis, Earth Surf. Process. Landforms, 38, 570–576, doi: 10.1002/esp.3302, 2013.

Pritchard, D., Roberts, G. G., White, N. J., and Richardson, C. N.: Uplift histories from river profiles, Geophys. Res. Lett., 36, L24301, doi:10.1029/2009GL040928, 2009.

Roberts, G. G., and White, N.: Estimating uplift rate histories from river profiles using African examples, J. Geophys. Res., 115, B02406, doi:10.1029/2009JB006692, 2010.

Roberts, G. G., White, N. J., Martin-Brandis, G. L., and Crosby, A. G.: An uplift history of the Colorado Plateau and its surroundings from inverse modelling of longitudinal river profiles, Tectonics, 31, TC4022, doi:10.1029/2012TC003107, 2012.

Royden, L. H, and Perron, J. T.: Solutions of the stream power equation and application to the evolution of river longitudinal profiles, J. Geophys. Res.- Earth Surface, 118, 497-518, 2013.

Royden, L. H, Clark, M. K, and Whipple, K. X.: Evolution of river elevation profiles by bedrock incision: analytical solutions for transient river profiles related to changing uplift and precipitation rates, EOS, Transactions of the American Geophysical Union81: Fall Meeting Supplement, Abstract T62F-09, 2000.

Rudge, J. F., Roberts, G. G., White, N. J., and Richardson, C. N.: Uplift histories of Africa and Australia from linear inverse modeling of drainage inventories, J. Geophys. Res.- Earth, 120, 894–914, doi:10.1002/2014JF003297, 2015.

Snyder, N. P., Whipple, K. X., Tucker, G. E., and Merritts, D. J.: Landscape response to tectonic forcing: Digital elevation model analysis of stream profiles in the Mendocino triple junction region, northern California, Geol. Soc. Am. Bull., 112, 1250–1263, 2000.

Snyder, N. P., Whipple, K. X., Tucker, G. E., and Merritts, D. J.: Channel response to tectonic forcing: field analysis of stream morphology and hydrology in the Mendocino triple junction region, northern California, Geomorphology, 53, 97 – 127, 2003.

Sorby, A. P, and England, P. C.: Critical assessment of quantitative geomorphology in the footwall of active normal faults, Basin and Range province, western USA, EOS, Transactions of the American Geophysical Union85: Fall Meeting Supplement, Abstract T42B-02, 2004.

Tarboton, D. G., Bras, R. L., and Rodriguez-Iturbe, I.: Scaling and elevation in river networks, Water Resour. Res., 25, 2037-2051, doi: 10.1029/WR025i009p02037, 1989.

Whipple, K. X.: Bedrock rivers and the geomorphology of active orogens, Annu. Rev. Earth Planet. Sci., 32, 151-185, doi: 10.1146/annurev.earth.32.101802.120356, 2004.

Whipple, K. X., and Tucker, G. E.: Implications of sediment-flux-dependent river incision models for landscape evolution, J. Geophys. Res.-Sol. Ea., 107, ETG3-1-ETG3-20, doi: 10.1029/2000JB000044, 2002.

Whipple, K. X., Wobus, C., Kirby, E., Crosby, B., and Sheehan, D.: New Tools for Quantitative Geomorphology: Extraction and Interpretation of Stream Profiles from Digital Topographic Data. Short Course presentedat the Geological Society of America Annual Meeting, Denver, CO, 2007.

Willett, S. D., McCoy, S. W., Perron, J. T., Goren, L., and Chen, C. Y.: Dynamic reorganization of river basins, Science, 343, 1248765,doi: 10.1126/science.1248765, 2014.

Wilson, J. W. P., Roberts, G. G., Hoggard, M. J., and White, N. J.: Cenozoic epeirogeny of the Arabian Peninsula from drainage modelling, Geochem. Geophys. Geosyst., 15, 3723–3761, doi:10.1002/2014GC005283, 2014.

Wobus, C., Whipple, K. X., Kirby, E., Snyder, N., Johnson, J., Spyropolou, K., Crosby, B., and Sheehan, D.: Tectonics from topography: Procedures, promise, and pitfalls, in: Tectonics, climate, and landscape evolution, edited by: Willett, S.D., Hovius, N., Brandon, M.T., and Fisher, D.M., GSA Special Paper, 398, Penrose Conference Series, 55–74, doi: 10.1130/2006.2398(04), 2006.

Yang, R., Willett, S. D., and Goren, L.: In situ low-relief landscape formation as a result of river network disruption, Nature, 520, 526-529, doi:10.1038/nature14354, 2015.

York, D.: Least squares fitting of a straight line with correlated errors, Earth Planet. Sci.Lett.,5, 320-324, doi:10.1016/S0012-821X(68)80059-7, 1968.

Table 1. Range of DW statistic and the related meaning

DW Statistic	Meaning
$0 \leq DW \leq D_L$*	Positivelyauto-correlated residuals
$D_L < DW \leq D_U$*	Beyond the suitability of Durbin-Watson test
$D_U < DW < 4\text{-}D_U$	Mutually independent residuals
$4\text{-}D_U \leq DW < 4\text{-}D_L$	Beyond the suitability of Durbin-Watson test
$4\text{-}D_L \leq DW \leq 4$	Negativelyauto-correlated residuals

*D_L and D_U represent the critical value of Durbin-Watson test and can be found in Durbin and Watson (1950).

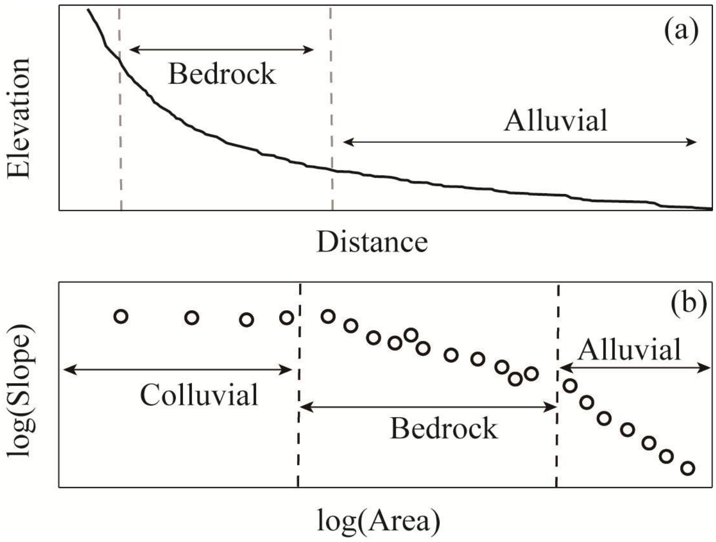

Figure 1. Schematic of a steady state river profile consisting of colluvial, bedrock and alluvial channels, revised from Figures 7A and B in Snyder et al (2000). (a) Stream profile. (b) Log-transformed slope-area plot.

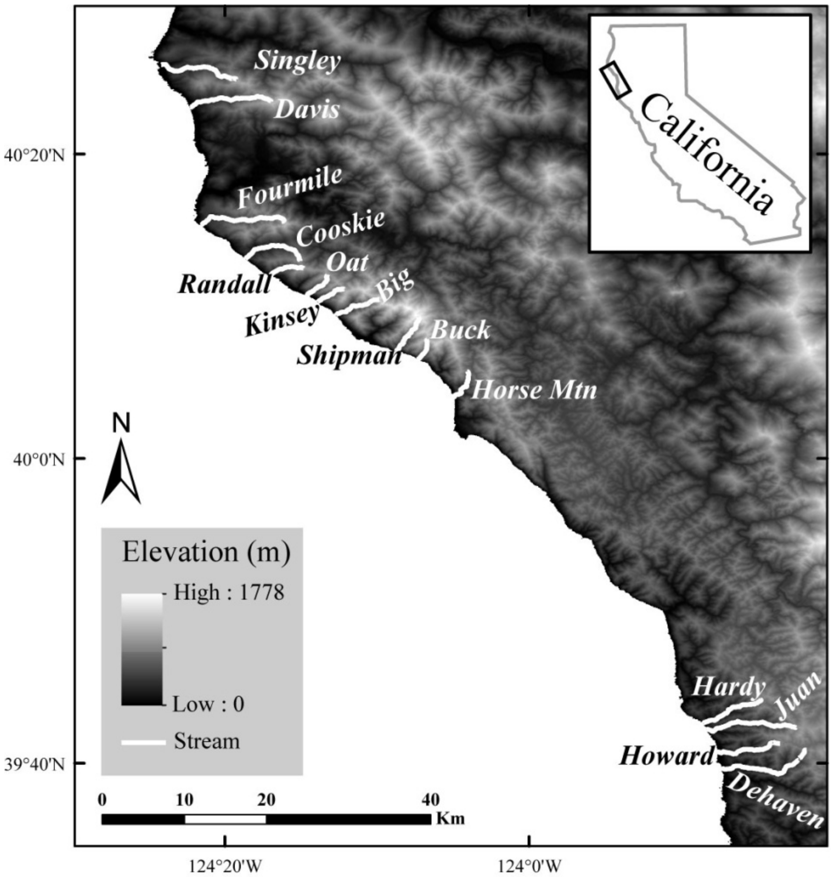

Figure 2. Streams in the Mendocino Triple Junction (MTJ) region of northern California, USA. Streams are from Snyder et al (2000). The elevation data are from 1 Arc-Second SRTM (http://earthexplorer.usgs.gov/)

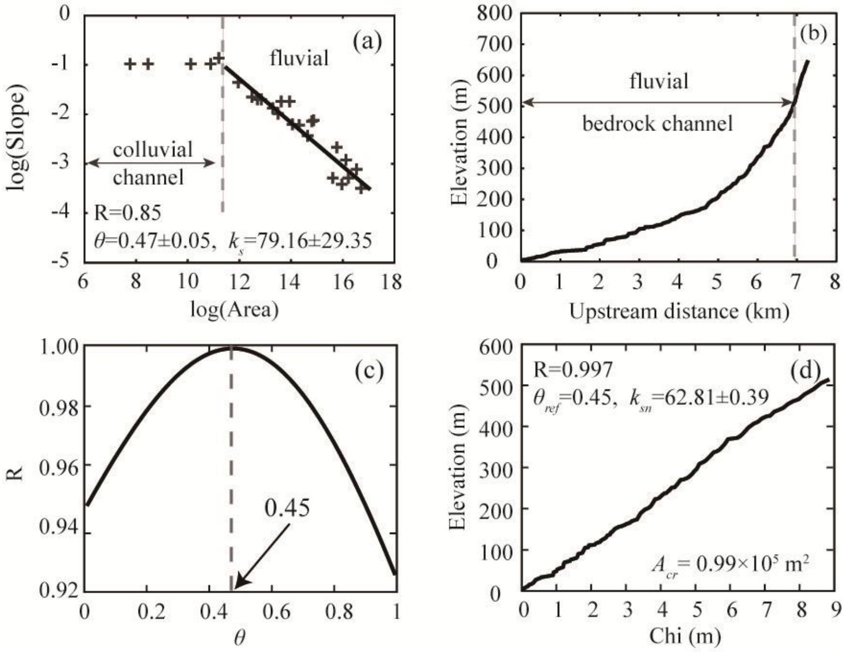

Figure3. Stream profile analysis of Cooskie. (a) Log-transformed slope-area plot. The slope was derived from the smoothed (horizontal distance of 300m) and re-sampled (elevation interval of 20m) elevation data. (b) The full river profile (without any smoothing or re-sampling) of Cooskie. (c) The correlation coefficients, R, as a function of θ for least-squares regression based on Eq. (3). The maximum value of R, which corresponds to the best linear fit, occurs at θ=0.45 (dotted line and black arrow). (d) χ-z plot of the bedrock channel profile, transformed according to Eq. (3) with θ=0.45, A_{cr}=0.1 km^2, and A_0=1 m^2.

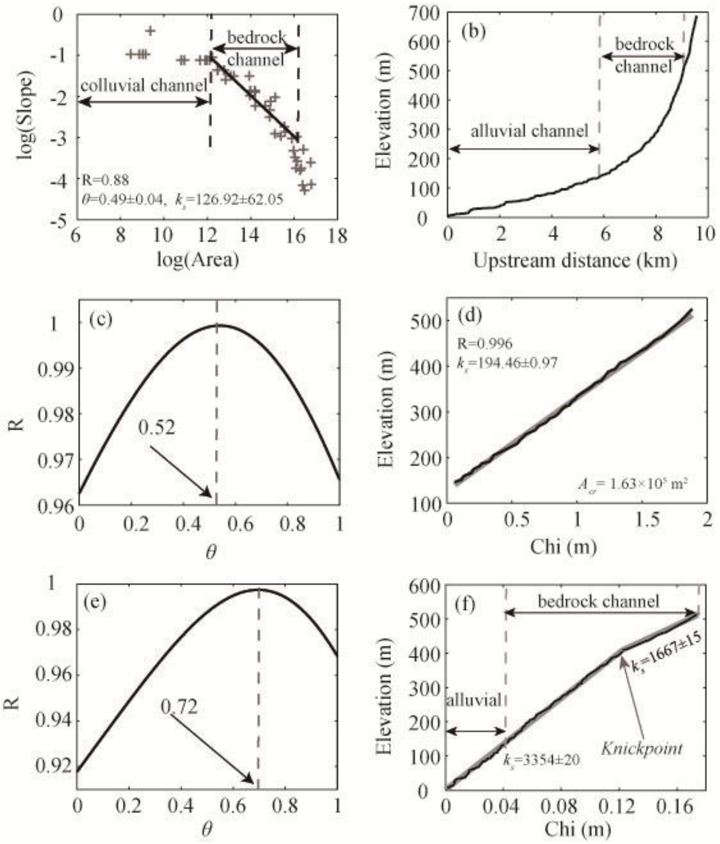

Figure 4. Stream profile analysis of Juan.(a) Log-transformed slope-area plot. The slope was derived from the smoothed (horizontal distance of 300m) and re-sampled (elevation interval of 20m) elevation data. (b) The full river profile (without any smoothing or re-sampling) of Juan. (c) The correlation coefficients of χ-z plots as a function of θ for the bedrock portion of the river. The maximum value of R occurs at θ=0.52. (d) χ-z plot of the bedrock channel profile based on a concavity value of 0.52. (e) The correlation coefficients of χ-z plots as a function of θ for fluvial (both bedrock and alluvial) channel. The maximum value of R occurs at θ=0.72. (f) χ-z plot of the fluvial (both bedrock and alluvial) channel profile based on a concavity value of 0.72.

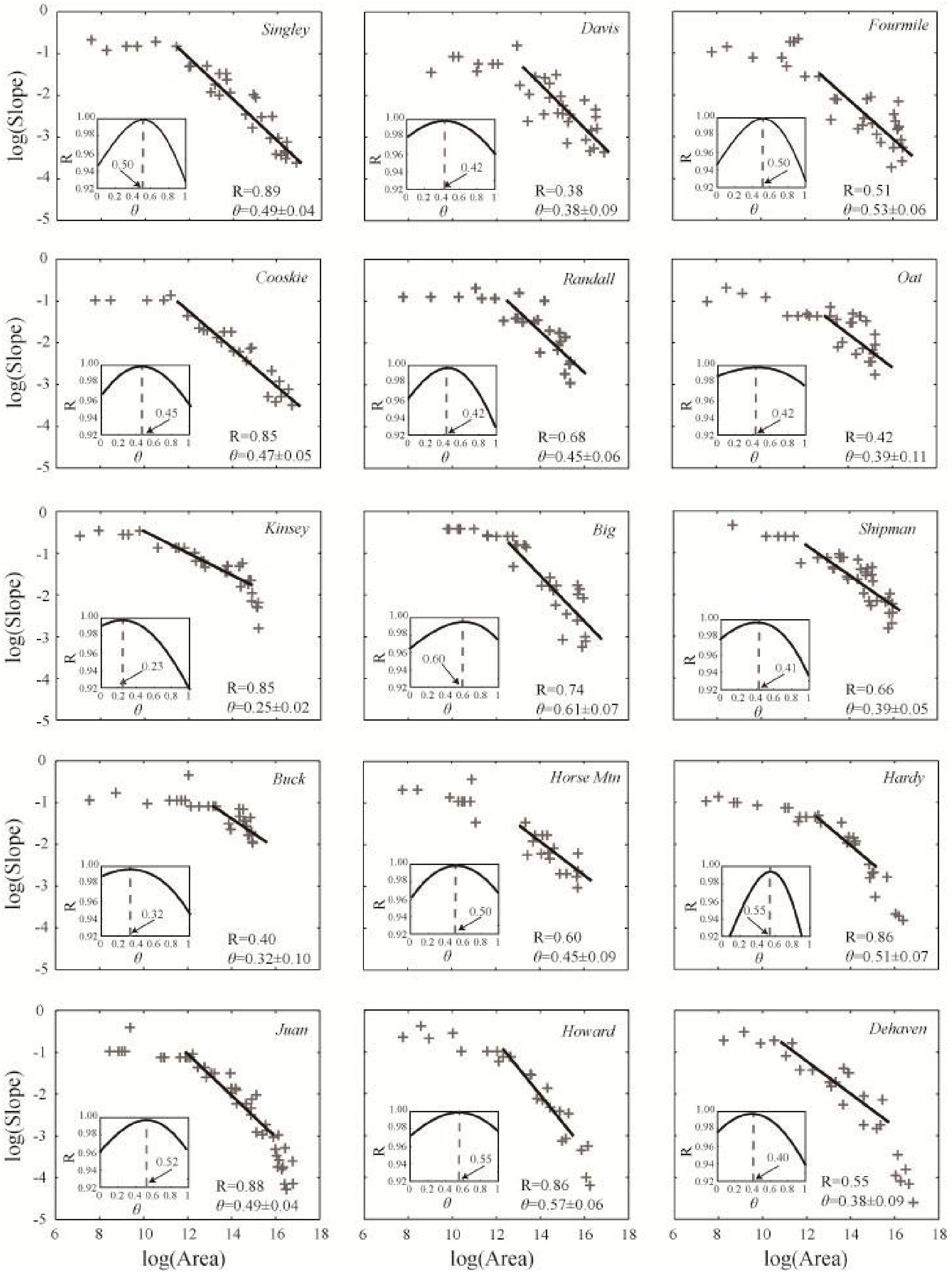

Figure5. Correlation coefficients derived from slope-area analysis and the integral approach. The slope was derived from the smoothed (horizontal distance of 300m) and re-sampled (elevation interval of 20m) elevation data. The correlation coefficients of χ-*z* plots as a function of *θ* for bedrock channels are shown in the left bottom. Then mean *θ* value is 0.45.

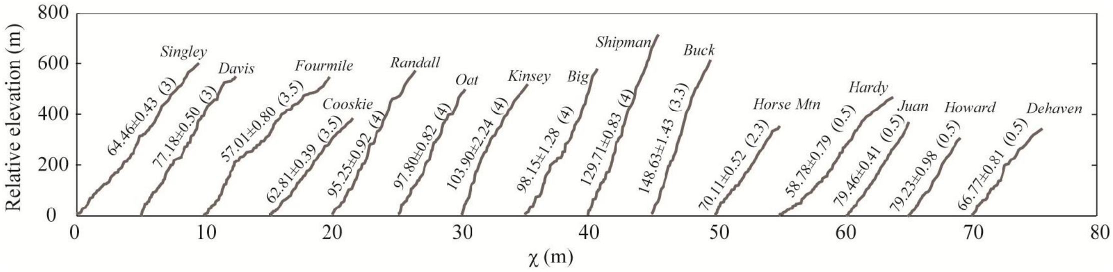

Figure 6.*χ-z* plots of the streams (bedrock channels) based on the mean concavity (0.45). Numbers are normalized channel steepness, k_{sn}, with the uncertainty estimates. Numbers in the parentheses are uplift rates with a unit of millimetre per year (Snyder et al., 2000). Italic characters are stream names.

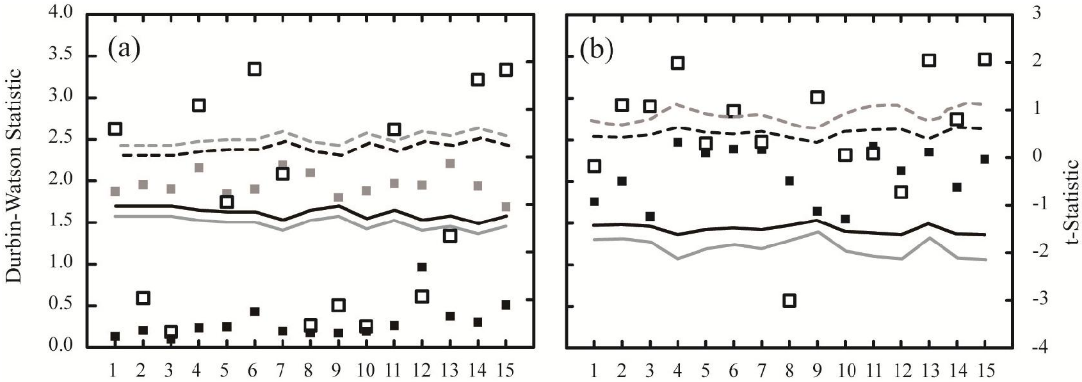

Figure 7. Statistic tests for the integral approach (a) and slope-area analysis (b). Black hollow squares are t-statistic of Spearman rank correlation coefficient. Black solid squares are Durbin-Watson statistics. The gray solid line, black solid line, black dashed line and gray dashed line are D_L, D_U, 4-D_u, and 4-D_L. Gray squares in Figure (a) are the Durbin-Watson statistics of revised χ-z plots. The river numbers 1 to 15 indicate streams: Singley, Davis, Fourmile, Cooskie, Randall, Oat, Kinsey, Big, Shipman, Buck, Horse Mtn, Hardy, Juan, Howard, and Dehaven.

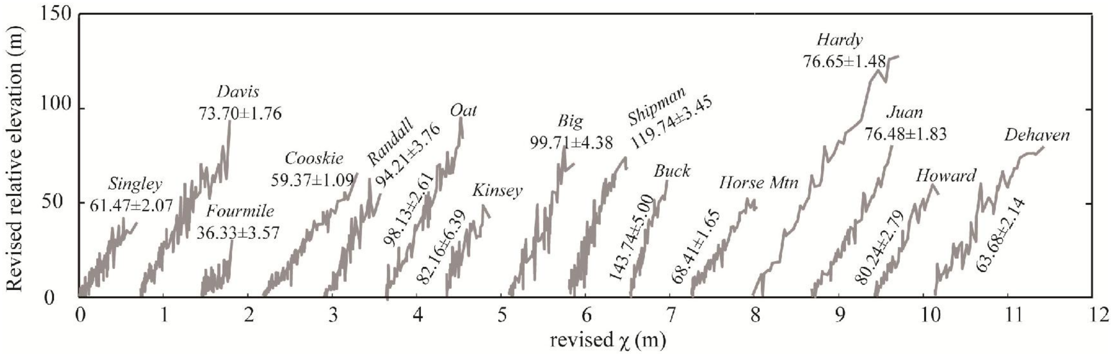

Figure 8. Revised relative elevation and χ values. Gray lines and Numbers are revised data and steepness index with uncertainty estimates.

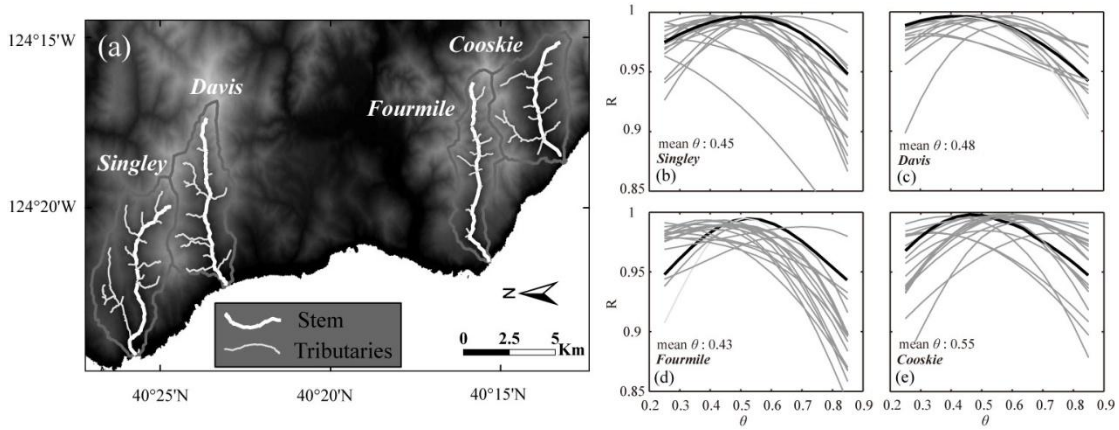

Figure9. Correlation coefficients of χ-*z* plots as a function of *θ*. (a) Location of the streams. (b-e) Correlation coefficients of χ-*z* plots based on a range of *θ* values. Black thick lines indicate stems.

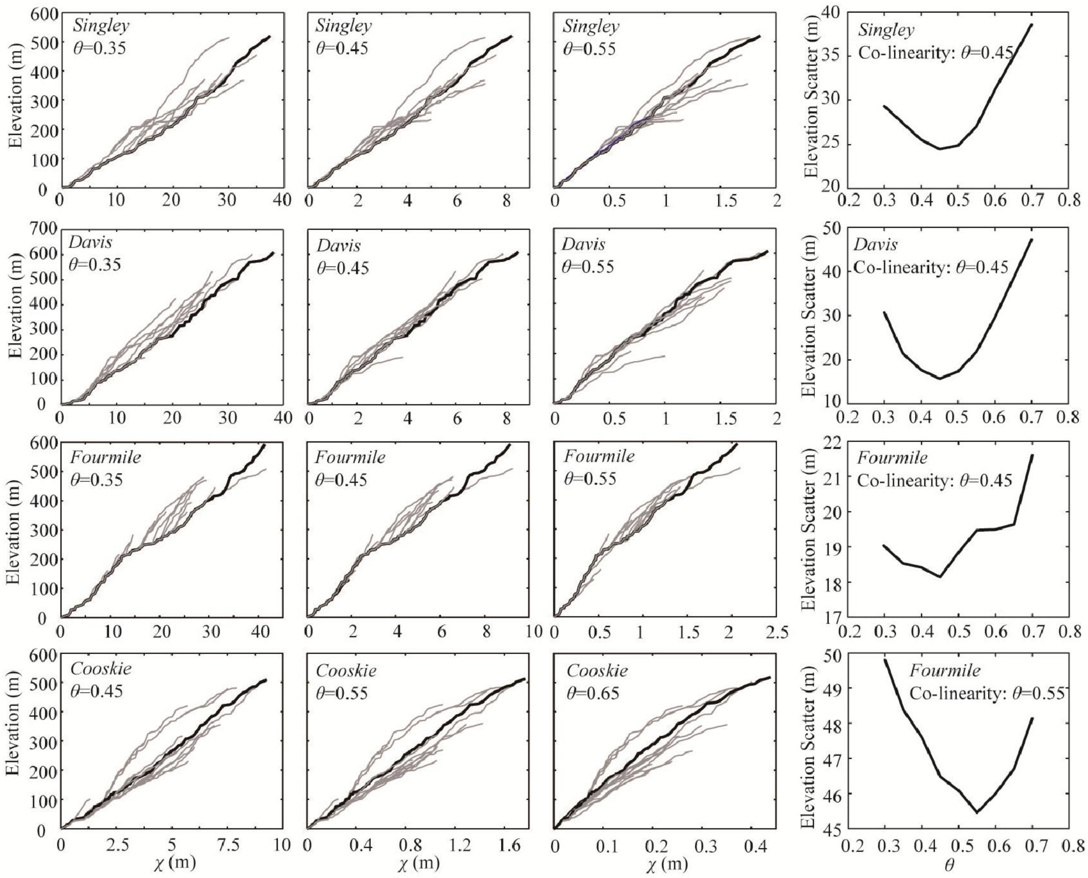

Figure10 Concavity values that maximize the co-linearity of the main stem with its tributaries. Black thick lines in the χ-*z* plots are stems.

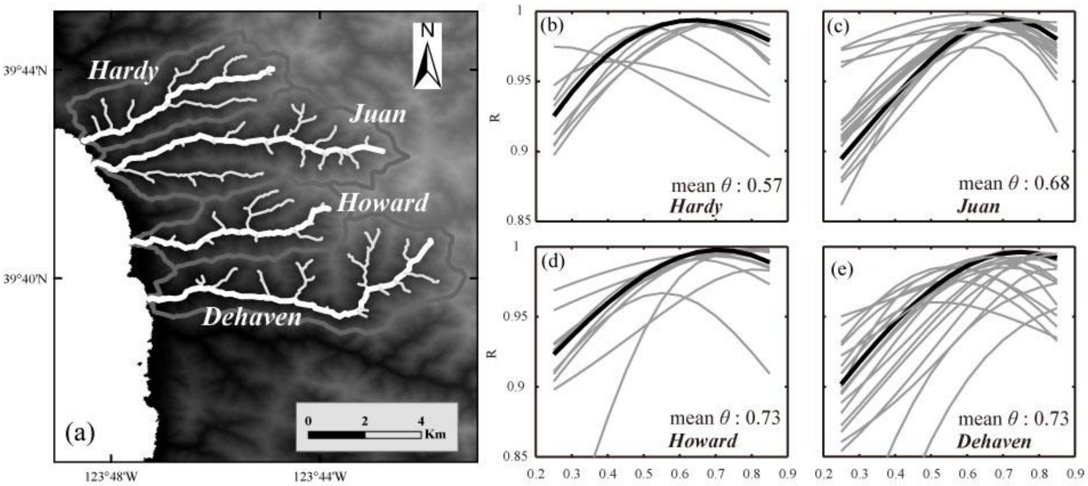

Figure11. Correlation coefficients of χ-*z* plots as a function of*θ*. (a) Location of the streams. (b-e) Correlation coefficients of χ-*z* plots based on a range of *θ* values. Black thick lines indicate stems.

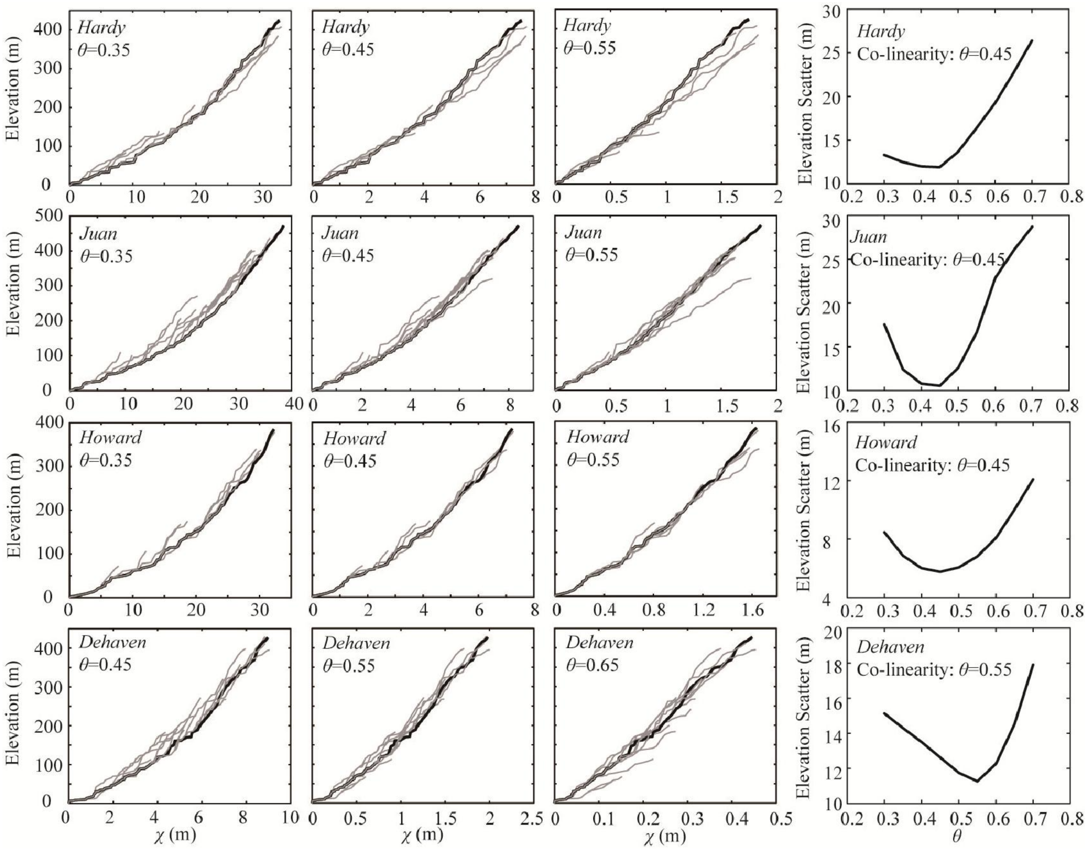

Figure12. Concavity values that maximize the co-linearity of the main stem with its tributaries. Black thick lines in the χ-*z* plots are stems.

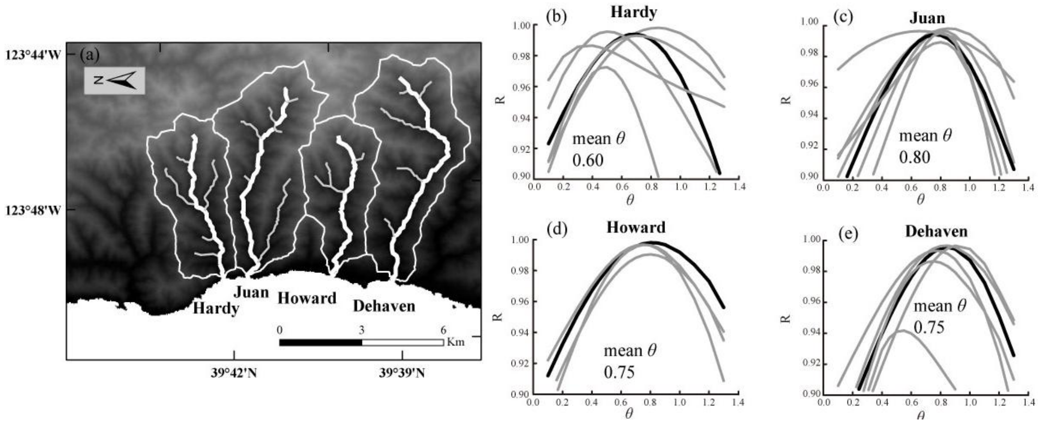

Figure13. Correlation coefficients of χ-z plots as a function of θ. (a) Location of the streams. Streams are extracted with a critical area of 0.5km^2. (b-e) Correlation coefficients of χ-z plots based on a range of θ values. Black thick lines indicate stems.

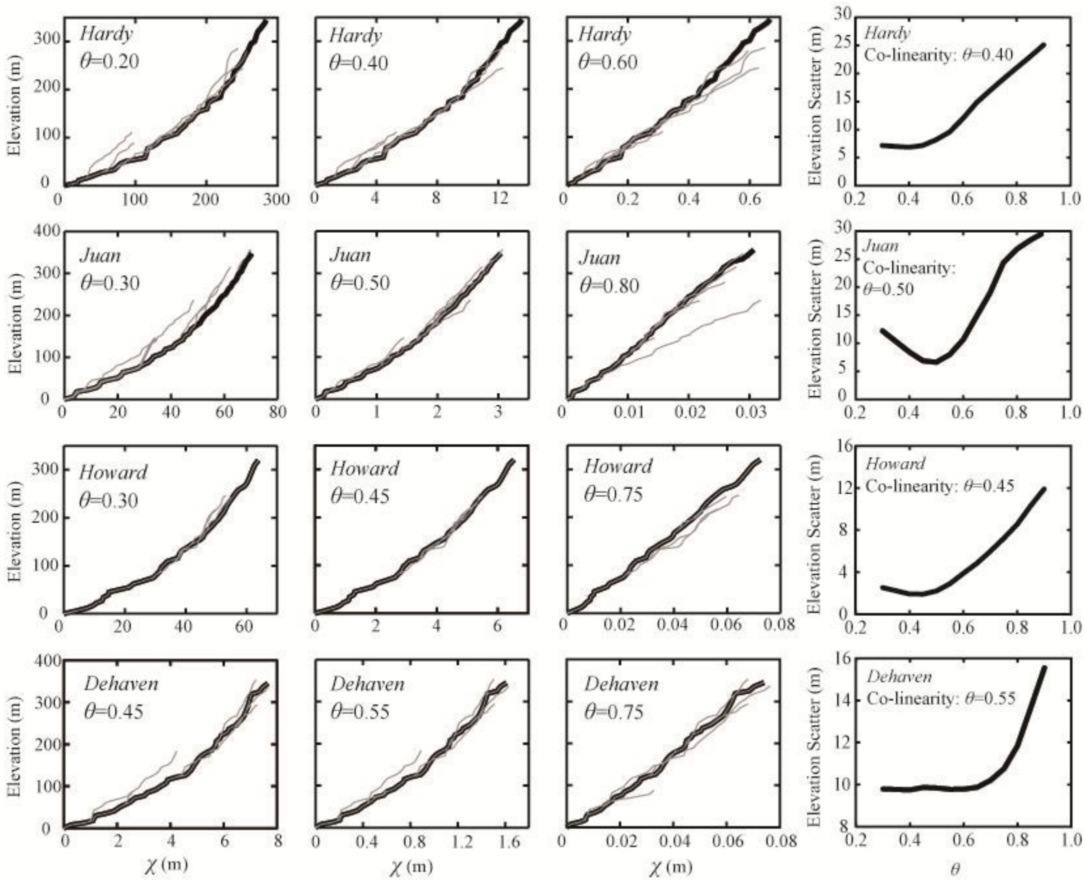

Figure14. Concavity values that maximize the co-linearity of the main stem with its tributaries. Black thick lines in the χ-z plots are stems.

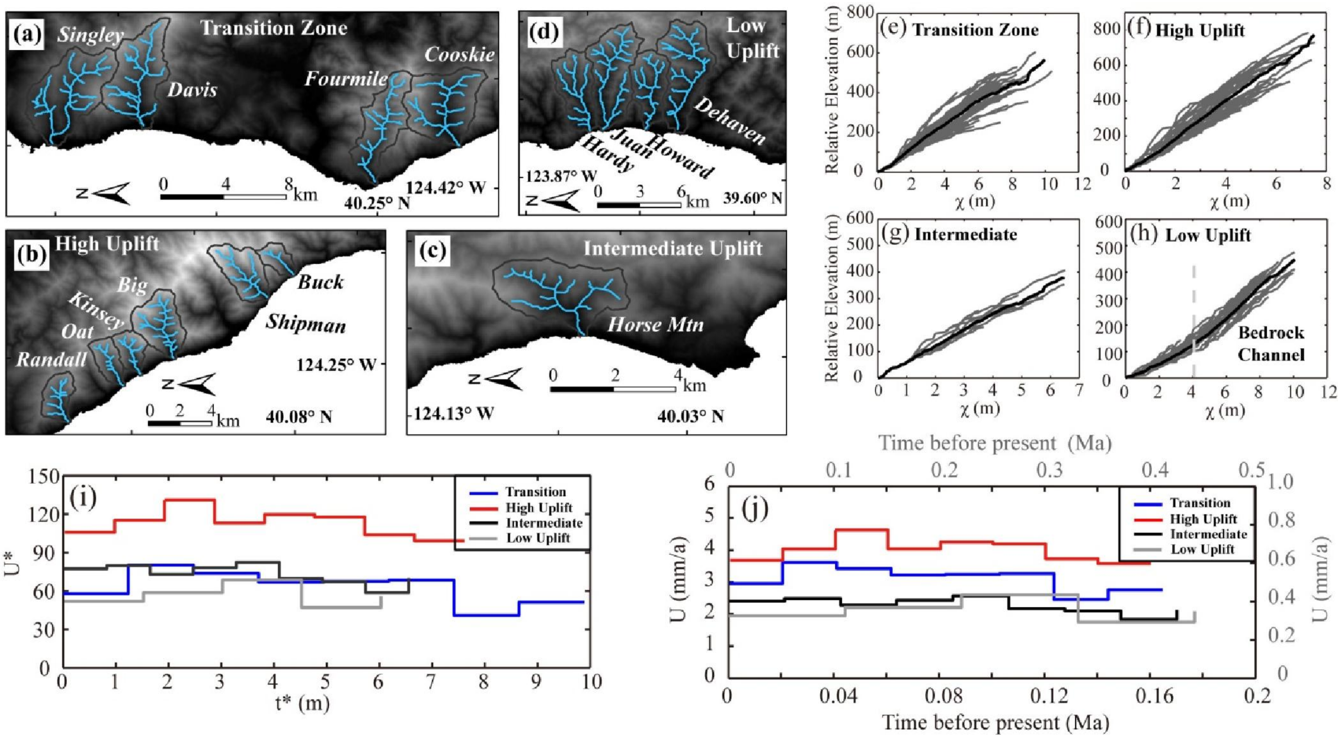

Figure 15. Uplift histories inferred from the stream profiles. (a)-(d) The map of streams in the four zones: north transition zone (a), King Range high-uplift zone (b), intermediate-uplift zone (c), and low-uplift zone (d). (e)-(h) The χ-*z* plots of the streams within each zone (A_0=1 m^2). The black line indicates an average result. (i) Scaled U*as a function of scaled time t*. (j) Inferred relative uplift rate as a function of time before the present. The left-bottom black axes show the results of north transition, high-uplift and intermediate-uplift zones. The right-top gray axes show the result of low-uplift zone.

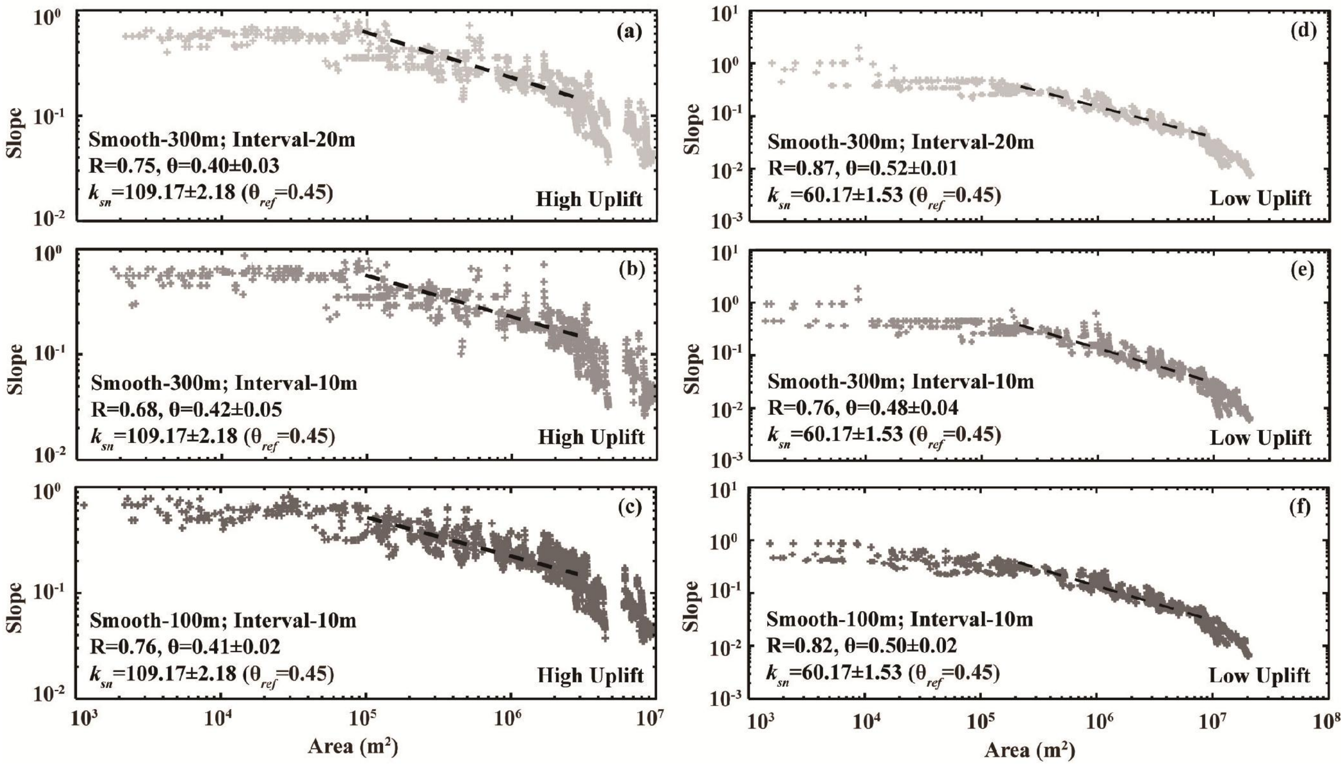

Figure 16. Log-transformed slope-area plots of streams in the high-uplift (a-c) and low-uplift (d-f) zones. Streams within the same zone are composited. The slope data are calculated via different methods: 300 m smoothing window and 20 m contour sampling interval (a and d), 300 m smoothing window and 10 m contour sampling interval (b and e), and 100 m smoothing window and 10 m contour sampling interval (c and f). Elevation data are from 1/3 arc-second USGS DEM (downloaded from https://catalog.data.gov/dataset/national-elevation-dataset-ned-1-3-arc-second-downloadable-data-collection-national-geospatial).

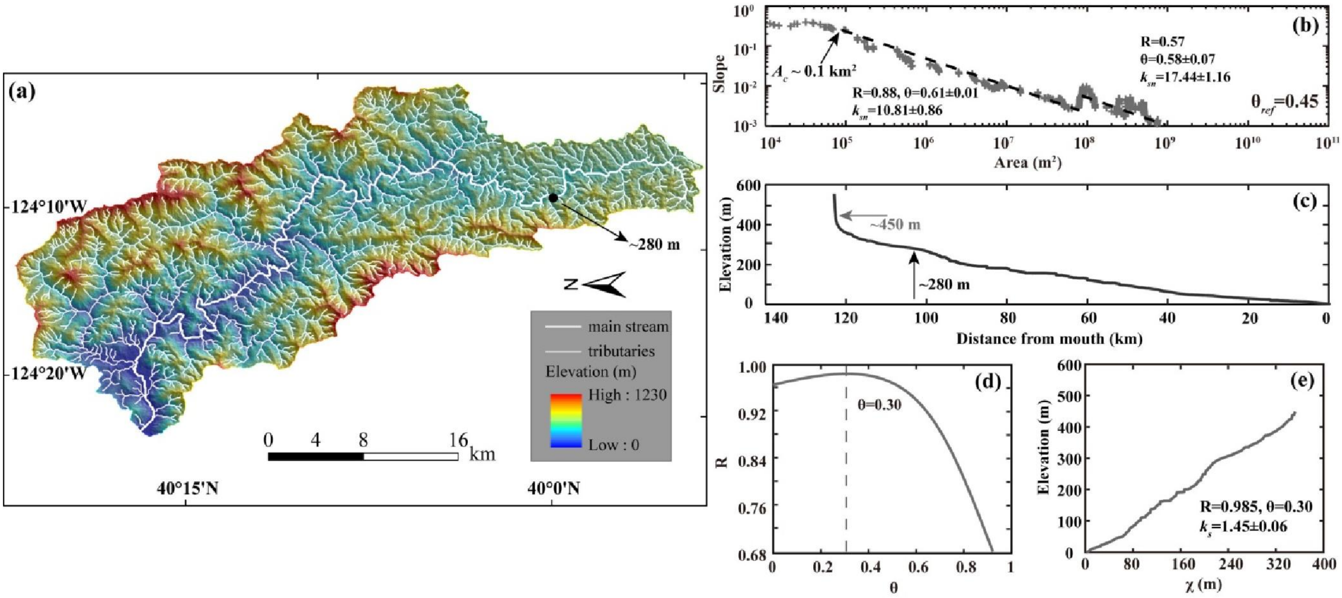

Figure 17. The slope-area data and χ-z plot of the stem of Mattole river. (a) Map of the stem and its tributaries in the Mattole drainage basin. Elevation data are from 1/3 arc-second USGS DEM (downloaded from https://catalog.data.gov/dataset/national-elevation-dataset-ned-1-3-arc-second-downloadable-data-collection-national-geospatial). (b) The log-transformed slope-area plot of the stem (300 m smoothing window and 20 m contour sampling interval). A knickpoint is detected from the plot with variant k_{sn} along the channel. (c) River profile of the stem. The gray arrow indicates the dividing point (~450 m) between the colluvial and fluvial portions. The black arrow shows the knickpoint (~ 280 m) on the stem. (d) The correlation coefficients between elevation and χ values as a function of θ. The maximum value of R, which corresponds to the best linear fit, occurs at θ=0.30 (gray dashed line). (e) The χ-z plot of the stem, transformed according to Eq. (3) with θ=0.30, A_{cr}=0.1 km^2, and A_0=1 m^2.

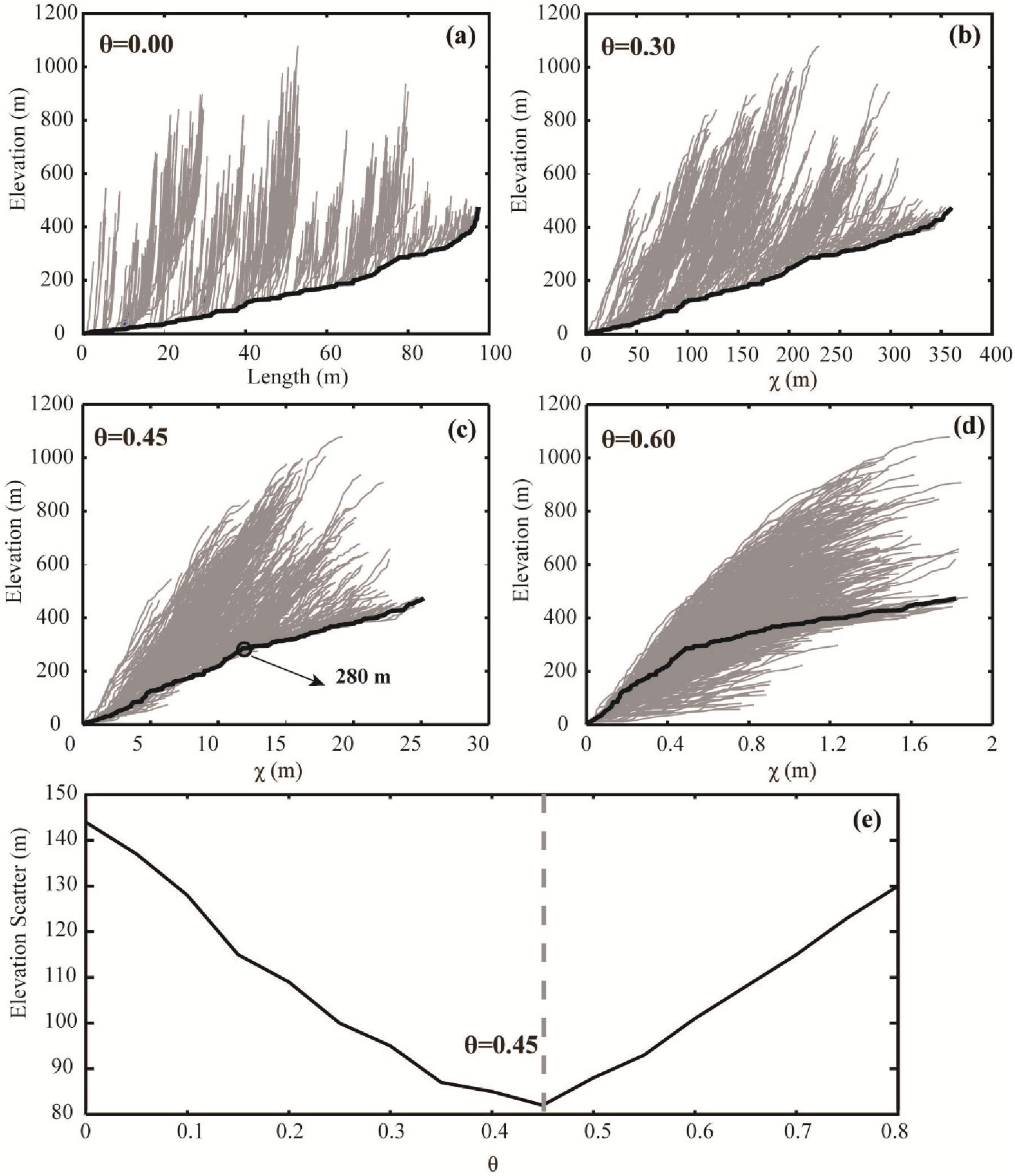

Figure 18.Concavity values that maximize the co-linearity of the main stem with its tributaries.(a)-(d) The χ-z plots of the stem (black line) and its tributaries (gray lines) using different values of θ (A_{cr}=0.1 km^2, and A_0=1 m^2). (e) The elevation scatter of the χ-z plots showing that minimum scatter is achieved with θ=0.45.

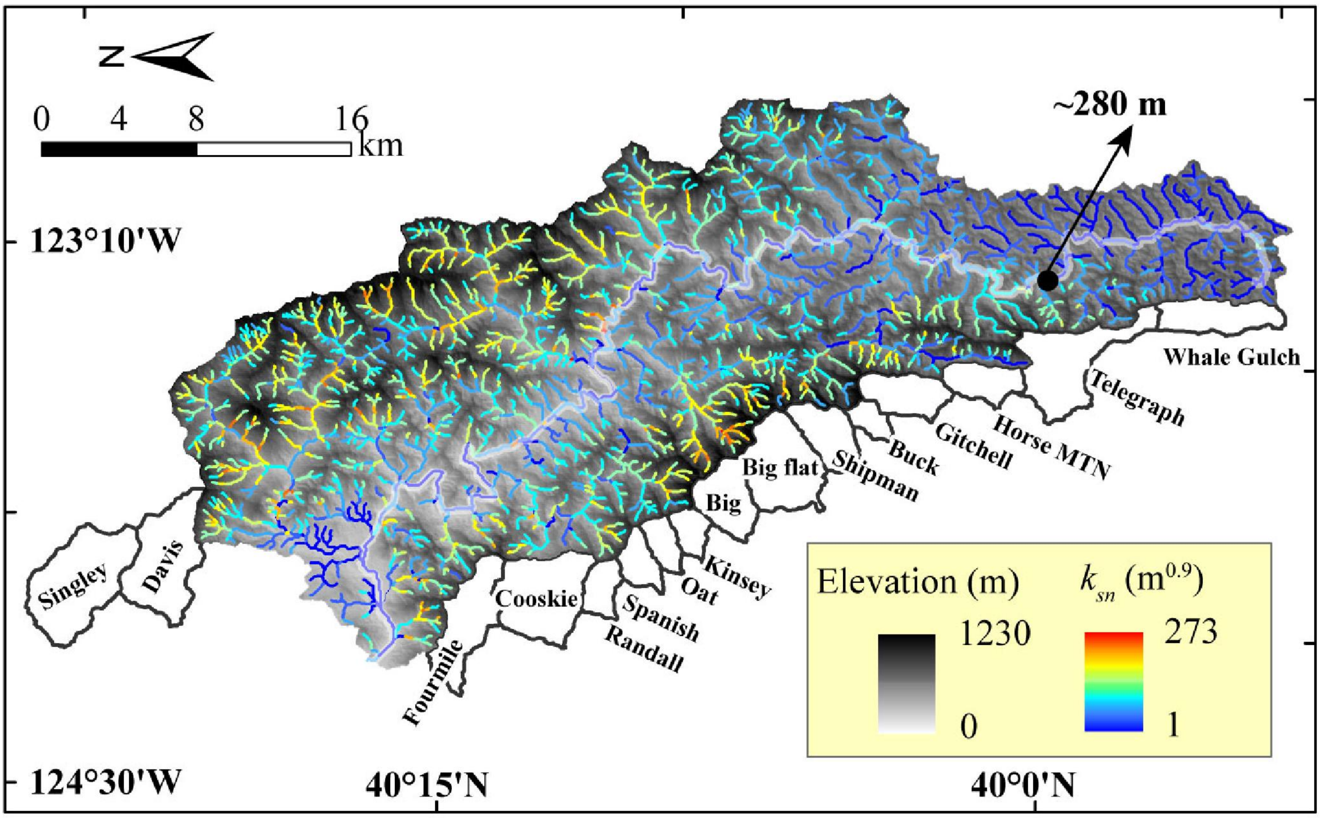

Figure 19. The map of k_{sn} (θ=0.45, elevation interval of 100 m) of the Mattole drainage basin. The black circle indicates the knickpoint on the stem. Low values are shown along the whole stem and its tributaries above the knickpoint. High k_{sn} values are distributed along the upstream of the tributaries below the knickpoint.